


Numerical examination of high-pressure fuel injection in common rail injector based on hydro-mechanical model

Cite as: Phys. Fluids **34**, 057114 (2022); <https://doi.org/10.1063/5.0091830>

Submitted: 17 March 2022 • Accepted: 04 May 2022 • Accepted Manuscript Online: 05 May 2022 • Published Online: 20 May 2022

 Zhuo Zhang (张卓), Ji-Wei Shi (史济伟), Xu-Liang Cheng (程旭亮), et al.



View Online



Export Citation



CrossMark

ARTICLES YOU MAY BE INTERESTED IN

[Improved fifth-order weighted essentially non-oscillatory scheme with low dissipation and high resolution for compressible flows](#)

Physics of Fluids **34**, 056105 (2022); <https://doi.org/10.1063/5.0090561>

[Drift of elastic floating ice sheets by waves and current: Multiple sheets](#)

Physics of Fluids **34**, 057113 (2022); <https://doi.org/10.1063/5.0091538>

[Pore-scale study of three-phase displacement in porous media](#)

Physics of Fluids **34**, 043320 (2022); <https://doi.org/10.1063/5.0089676>



Physics of Fluids

Special Topic: Paint and Coating Physics

Submit Today!

Numerical examination of high-pressure fuel injection in common rail injector based on hydro-mechanical model

Cite as: Phys. Fluids **34**, 057114 (2022); doi: 10.1063/5.0091830

Submitted: 17 March 2022 · Accepted: 4 May 2022 ·

Published Online: 20 May 2022



View Online



Export Citation



CrossMark

Zhuo Zhang (张卓), Ji-Wei Shi (史济伟), Xu-Liang Cheng (程旭亮), Yan-Jun Dai (戴艳俊), and Wen-Quan Tao (陶文铨)^{a)}

AFFILIATIONS

Key Laboratory of Thermal-Fluid Science and Engineering of MOE, School of Energy and Power Engineering, Xi'an Jiaotong University, Xi'an 710049, People's Republic of China

^{a)} Author to whom correspondence should be addressed: wqtao@mail.xjtu.edu.cn

ABSTRACT

The design of a high-pressure common rail injector is critical to the efficient operation of a high-power internal combustion engine. In this study, we develop a one-dimensional model of a hydro-mechanical system to examine the dynamic behavior of the injector. We use the validated model to investigate the effects of the operating conditions and internal structural parameters on the rate of injection, and analyze its dynamic response under single- and multi-injection conditions. The results show that the rail pressure and energizing time have different effects on the delays in opening and closing, and a sufficiently long energizing time is needed to lift the needle to a fully open position. A smaller semi-angle of the seat of ball valve might initiate faster injection. The diameter of the hole, half-angle of the seat, and half-angle of the cone of the needle valve all have positive effects on the rate of injection. The critical dwell time increased with the rail pressure under an energizing time of 0.5 ms, while the opposite result is obtained under energizing times of 1.0, 1.5, and 2.0 ms.

Published under an exclusive license by AIP Publishing. <https://doi.org/10.1063/5.0091830>

NOMENCLATURE

A	Area (m^2)
B	Bulk modulus (Pa)
C_q	Discharge coefficient
d, D	Diameter (m)
f	Friction factor
F	Force (N)
h	Clearance spacing (m)
k	Elastic constant (N m^{-1})
l, L	Length (m)
m	Mass (kg)
m', M	Auxiliary parameter 1
p	Pressure (Pa)
q, Q	Volume flow rate ($\text{m}^3 \text{s}^{-1}$)
Re	Reynolds number
$taux$	Auxiliary parameter 2
v	Velocity (m s^{-1})
V	Volume (m^3)

x Displacement or lift (m)

Greek letters

α	Auxiliary angle ($^\circ$) the half-angle of the seat of the needle valve
β	Auxiliary parameter 3
ε	Absolute roughness (m)
θ	Semi angle of the seat ($^\circ$)
λ	Theoretical Reynolds number
μ	Dynamic viscosity (Pa s)
ρ	Fuel density (kg m^{-3})
σ	Half-angle of needle cone ($^\circ$)

Subscripts and superscripts

a	Active
b	Ball
c	Contact, cone
cri	Critical value

h	Hydraulic
pop	Poppet
qmax	Maximum discharge coefficient
visc	Viscous

I. INTRODUCTION

The growing number of vehicles with diesel engines has increased environmental pollution, and the automotive industry has made significant efforts to reduce the environmental impact of diesel engines over the past few years.^{1,2} The fuel injection system is a key technology that determines fuel efficiency and emissions.^{3,4} Its performance in the context of the law of fuel injection, fuel distribution in the cylinder, and speed of fuel injection is a decisive factor in the products of atomization, combustion, and emission in the cylinder of a diesel engine. The high-pressure common rail injection system (HPCRIS) plays a vital role in fuel injection technologies.

The importance of optimization of the HPCRIS makes it critical to establish a mathematical model that allows for fast and flexible changes in the relevant parameters. It provides a preliminary range of structural parameters for the modular design of the entire system, shortens the design time, and reduces cost. Pogulyaev *et al.*⁵ developed a mathematical model of hydrodynamic processes of the high-pressure common rail fuel injection system (third generation) designed by the firm Bosch. It can be used for studying and optimizing fuel supply systems of the given type. Zhang *et al.*⁶ established one-dimensional (1D) models of a common rail system and a multi-pump pressure reservoir-based fuel injection system in AMESim software to study the effects of different structures and geometric parameters on pressure fluctuations. Wang *et al.*⁷ proposed a mathematical model of the HPCRIS that contains three sub-systems: models of a high-pressure pump, a common rail, and the injector. They also designed a model-free controller, called the extended state observer-based intelligent proportional integral (ESO-based IPI) controller, for the HPCRIS considered.

The fuel injector is the most critical and complex of the major components of the HPCRIS (the others being the electronic control unit, high-pressure oil pump, and common rail pipe). Many researchers have thus investigated it. Patil and Sahu⁸ experimentally investigated the spray characteristics of a novel twin-jet cross-stream airblast injector. They focused on the effects of annular air swirl within the injector on the characteristics of the droplets and their dispersion. Reid *et al.*⁹ carried out visualization tests on cavitating flow structures at a range of pressures of up to 2050 bar in real-scale flow geometry. This enabled their behavior to be observed across the complete range of working pressures of currently used common rail systems. In addition to fuel injection, the injector uses fuel, a fluid with low compressibility, to realize the opening and closing of internal mechanical components. The principle of it is based on Pascal's law in hydrostatics.^{10,11} Many researchers have developed 1D models of the injector and analyzed its dynamic response to reveal the complex hydrodynamic behaviors inside it. Rahim *et al.*¹² used a 1D model to study the effects of temperature on the performance of a four-cylinder engine, and Pogulyaev *et al.*⁵ developed a mathematical model of a common rail piezoinjector. The simulated total injected masses per cycle of both were in good agreement with experiment results.

The properties of fuel and the internal structural parameters of the injector affect the injection process. The density, bulk modulus,

and dynamic viscosity of the fuel all change with the pressure. There are many research studies on the physical properties of fuel.^{13–15} Kim *et al.*¹⁶ investigated the effects of the viscosity and density of fuel on the rate of injection. The variation in temperature was considered by Salvador *et al.*¹⁷ and Payri *et al.*,¹⁸ who used the hypothesis of adiabatic flow. Salvador *et al.*¹⁹ studied the influence of using biodiesel fuels on the hydraulic behavior of a solenoid-operated common rail injection system based on a 1D model. A modification in the hardware of the injector was proposed so that it delivered similar performance when using biodiesel to that of the original injector configuration when using standard diesel fuel. Hu *et al.*²⁰ studied the impact of structural parameters on the dynamic response of an electronic fuel injector, and Bai *et al.*²¹ established the rules of influence of various parameters on the volume of fuel injected.

Although several 1D models have been proposed in the literature, few provide details of the different components of the injector, especially its hydraulic part: the ball valve and the needle valve. The effects of parameters related to the ball valve and the needle valve (like the semi-angle of the seat of the ball valve, diameter of the hole of the needle valve, half-angle of the seat of the needle valve, and half-angle of the needle cone) have also been seldom studied. Important uncertainties thus persist regarding the influence of the valve-related parameters on the hydraulic behavior of the injector. In this study, we provide detailed mathematic models of the injector and perform simulations based on a code that we wrote. The displacement of the needle, rate of injection, and pressure in control volume (CV) under different injection pressures and energizing times (ETs) are studied. The effects of geometrical parameters near the location of the valve are investigated, and the critical dwell time (the time needed between injections to ensure stable operation) under a multi-injection condition is considered. This paper highlights the well-illustrated mathematic model of the injector, which is not shown in most similar literatures. To the author's knowledge, this is the first time to obtain the variation law of critical time with pressure and energizing time. In addition, the comparison of two kinds of pipeline sub-models (1D pipeline model and lumped parameter pipeline model) is conducted, which is not seen in other studies. The results can provide theoretical guidance for the design and optimization of the injector. In the following, the proposed numerical model is detailed in Sec. II. Section III describes and analyzes the results of the dynamic behavior of the injector, and some conclusions are drawn in Sec. IV.

II. METHODOLOGY

A. Model assumptions

The following assumptions are made regarding the model:

- (i) Complex electromagnet elements are replaced by the electromagnetic force, which is directly applied to control the ball valve.
- (ii) Because the injection cycle is very short, the variation in temperature is omitted. The properties of fuel at 40 °C are considered and depend only on the pressure.
- (iii) Considering the stiffness of the shell of the injector, the wall is regarded as rigid.
- (iv) Only the force along the axis of the injector is considered.
- (v) All pipelines in the injector are assumed to have a circular section. Fuel flow in the pipe is simplified to 1D flow.

B. Description of sub-models

The mathematic model of an injector consists of several sub-components, including the mass block, pipeline, orifice, hydraulic chamber, leakage flow, ball valve, and needle valve, as shown in Fig. 1. The coupling of these elements needs to satisfy the law of energy conservation.²¹ Before describing each sub-model, the operation of the fuel injector is introduced as follows:

Initially, high-pressure fuel fills the internal high-pressure space, including pipelines 1/2/4, chambers 1/3/5/6, and the control volume. When the solenoid coil is energized to take the ball valve off its seat, the high-pressure fuel flows quickly out of the control volume through the oil outlet (OA) orifice. As the rate of flow at the outlet of the OA orifice is higher than that at the inlet of the oil inlet (OZ) orifice, pressure in the control volume begins to decrease. Then, under the upward force from chambers 5/6, the command rod and the body of the needle valve move upward. High-pressure fuel flows from chamber 6 to the oil sac (SAC) chamber and is eventually ejected from the orifice of the nozzle. While the above describes the initiation of fuel injection, its termination consists of this procedure in reverse. The electromagnetic force disappears, the ball valve is closed, the pressure in the control volume is restored, and the needle valve is seated to end fuel injection.

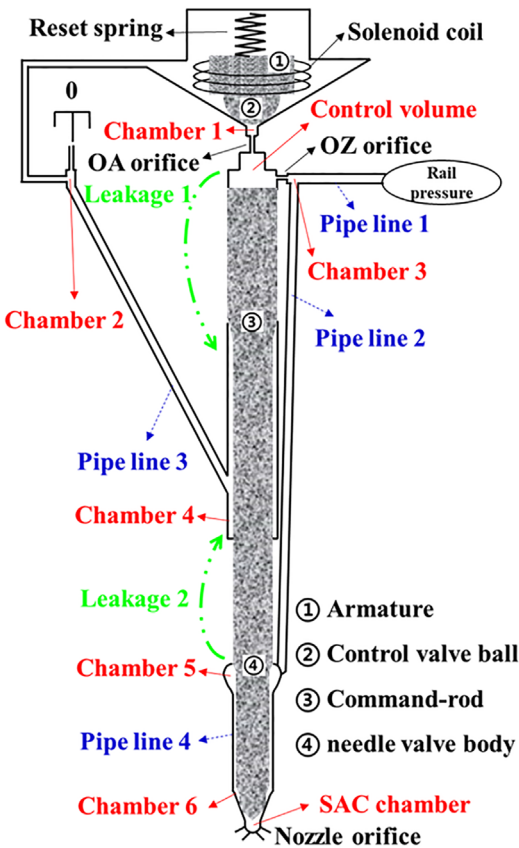


FIG. 1. 2D schematic of internal structure of the injector.

1. Mechanical sub-model

A mechanical sub-model is used to describe the movement of the components of the injector. We use two mechanical sub-models (M_1 and M_2) to represent two moving parts. The armature and control ball valve are represented by M_1 . They are considered to be rigidly connected and thus treated as a whole. Similarly, the command rod and body of the needle valve are represented by M_2 . The governing equation of the mechanical sub-model is as follows:

$$mx'' + kx = F_{ele} + F_{visc} + \sum_i p_i A_i, \quad (1)$$

where m (kg) is the mass, x (m) is the displacement, k ($N\ m^{-1}$) is the elastic constant, and F (N) is the net force applied to the mass along the axis of the injector.²² For M_1 , the force on mass m_1 includes the pre-tightening spring force, electromagnetic force, and hydraulic pressure from the chambers 1 and 2. For M_2 , the force includes hydraulic pressure from the control volume, chambers 4–6, the SAC chamber, and the viscous force of the leaking fuel, as shown in Fig. 1. These forces are calculated by the other sub-models and used as input to calculate the displacement of the block. For example, the viscous forces are computed by the leakage flow sub-model, which is described in Sec. II B 5. The parameters of M_1 and M_2 in Eq. (1) are shown in Table I.

2. Sub-model of pipeline

To describe high-pressure fuel flow in a 1D pipe, the equations of continuity and momentum are used as follows:

$$\frac{\partial \rho}{\partial t} + \frac{\partial(\rho v)}{\partial x} = 0, \quad (2)$$

$$\frac{\partial(\rho v)}{\partial t} + \frac{\partial(\rho v^2 + p)}{\partial x} + \frac{f \rho v |v|}{2D} = 0, \quad (3)$$

where D (m) is the diameter of the pipeline, ρ ($kg\ m^{-3}$) is the density of the fluid, and v ($m\ s^{-1}$) is the velocity of its flow through the pipe. The sub-model is based on a 1D mesh that considers the compressibility and inertia of the fluid. The pressures, densities, and flow rates are computed at each interior point. The set of partial differential equations is integrated both in time and space, and the time steps need to be carefully determined.

The above 1D pipeline model often requires a long central processing unit time to solve. A sub-model of lumped parameters can be used as a reasonable alternative. The drop in the pressure of fluid flowing through the pipe can be calculated by the following formula:

$$\Delta p = f \frac{L}{D} \frac{\rho v^2}{2}, \quad (4)$$

where f is the friction factor and L (m) is the length of the pipe. Equation (4) can be regarded as a simplification of Eq. (3). The friction factor f can be calculated as²³

$$f = \begin{cases} \frac{64}{Re}, & Re < 2000, \\ \left(\frac{1}{-2.0 \log \left(\frac{\epsilon/D}{3.7} + \frac{2.51}{Re f^{1/2}} \right)} \right)^2, & Re > 2000, \end{cases} \quad (5)$$

where ϵ (m) is the absolute roughness and Re is the Reynolds number. Our injector model has four main pipelines, as shown in Fig. 1, and

TABLE I. Model parameters.

Parameter	Value	Unit
Mass (m) of M_1/M_2	0.012/0.021	kg
Diameter (D) of pipeline 1/2/3/4	0.0025/0.002/0.0013/0.0022	m
Length (L) of pipeline 1/2/3/4	0.3/0.054/0.052/0.023	m
Absolute roughness (ε) of pipeline 1–4	0.000 01	m
Diameter (d_d) of OZ/OA/nozzle/return oil orifice	0.2585/0.32/0.31/3	mm
Maximum flow coefficient (C_{qmax}) of OZ/OA/nozzle/return oil orifice	0.7/0.8/0.8/0.7	
Critical flow number (λ_{crit}) of OZ/OA/nozzle/return oil orifice	1000/1000/1000/1000	
Dead volume (V_0) of chambers 1/2/3/4/5/6, control volume, and SAC chamber	0.24/20/163/150/100/3.84/11.33/1.54	mm ³
Clearance spacing (h) of leakage 1/2	0.00175/0.00175	mm
Contact length (l_c) of leakage 1/2	24.7/15	mm
Seat semi-angle of the ball valve (θ)	60	°
Seat diameter of the ball valve (d_s)	0.45	mm
Ball diameter of the ball valve (d_b)	1.33	mm
Maximum flow coefficient of the ball valve ($C_{qmax,ball}$)	0.7	
Critical flow number of the ball valve ($\lambda_{crit,ball}$)	100	
Diameter of poppet of needle valve (d_{pop})	2.2	mm
Diameter of the cone of needle valve (d_c)	1.6	mm
Diameter of the hole of needle valve (d_e)	1.6	mm
Seat half-angle of needle valve (σ)	29.6	°
Needle cone half-angle of needle valve (α)	29.9	°
Maximum flow coefficient of ball valve of needle valve ($C_{qmax,needle}$)	0.9	
Critical flow number of ball valve of needle valve ($\lambda_{crit,needle}$)	1000	

their parameters are listed in Table I. We use the lumped parameter sub-model for all four pipelines and analyze the effects of different sub-models of the pipeline on the results.

3. Sub-model of orifice

There are four characteristic orifices in our injector model: the OA orifice, OZ orifice, orifice of the nozzle, and orifice of the outlet for the returning oil. The drop in the pressure of fuel through the orifice is related to the flow rate as follows:

$$q = C_q \times A \times \sqrt{\frac{2|\Delta p|}{\rho}} \times \text{sign}(\Delta p), \quad (6)$$

$$C_q = C_{qmax} \times \tanh\left(\frac{2\lambda}{\lambda_{crit}}\right), \quad (7)$$

$$\lambda = \frac{\rho d_h}{\mu} \times \sqrt{\frac{2|\Delta p|}{\rho}}, \quad (8)$$

where C_q is the discharge coefficient, λ is called the theoretical Reynolds number, Δp (Pa) is the difference in pressure between upstream and downstream of the orifice, d_h (m) and A (m²) are the hydraulic diameter and the sectional area, respectively, and ρ (kg m⁻³) and μ (Pa s) are the density and dynamic viscosity of the fuel, respectively. They are calculated using the average value of the upstream and downstream pressures, as described in the sub-model for the properties of fluid. In addition to its geometric dimensions, λ_{crit} (critical

theoretical Reynolds number) and C_{qmax} (maximum discharge coefficient) are the key parameters determining the discharge coefficient of each orifice.

4. Sub-model of hydraulic chamber

The volume of the control chamber (or control volume, CV) changes with the displacement of the needle. The pressure inside it is significant for the dynamics of the needle and is dependent on the variation in volume. There are six other chambers in the path of fuel flow, as shown in Fig. 1 (schematic diagram only; not drawn to scale). The pressures in all these chambers need to satisfy the following formula:

$$\frac{V}{B} \frac{dp}{dt} + \frac{dV}{dt} = \sum Q_i, \quad (9)$$

where Q_i (m³ s⁻¹) is the volumetric flow rate at the inlet or outlet, V (m³) is the volume of each chamber, and B (Pa) is the bulk modulus of the fluid. It is calculated based on the chamber pressure as described in the sub-model of the properties of the fluid. The rate of change in volume caused by moving part as represented in the above equation can be calculated as follows:

$$\frac{dV}{dt} = A \cdot v, \quad (10)$$

where A (m²) is the cross-sectional area of the moving element and v is its velocity. The dead volume V_0 of each chamber, which represents the minimum volume of the chamber, is also needed to calculate V .

5. Sub-model of leakage flow

Due to the difference in pressure, static leakage occurs at the clearance between the control–piston couple and the nozzle–needle valve couple. The high-pressure fuel in the injector leaks to the low-pressure chamber and then flows to the tank through the return line. As shown in Fig. 1, there are two leakage flows in the model: from the control volume to chamber 4 and from chamber 5 to chamber 4. Without considering eccentricity, the sectional zone between the moving part (command rod and needle) and housing of the injector can be regarded as a standard annular area. Then, the analytical solution of Couette–Poiseuille flow can be used to determine the leakage flow rate

$$q = -\frac{\Delta p}{12\mu l_c} h^3 \pi d_1 + \frac{v}{2} h \pi d_1 \tag{11}$$

$$F_{\text{visc}} = -\frac{\Delta p}{2} \pi d_1 h + \mu l_c v \pi \frac{d_1}{h} \tag{12}$$

where Δp (Pa) is the difference in pressure between the upstream and the downstream of the clearance, l_c (m) is the contact length, h (m) is the clearance spacing, d_1 (m) is the diameter of the moving part, and v (m/s) is its velocity. F_{visc} (N) is its viscous resistance force, which will be used in later calculations.

6. Sub-model of ball valve

During the lifting and lowering of the ball valve, fuel flows through it under the action of the pressure difference, and a certain hydraulic pressure acts on the ball valve as shown in Fig. 2(a). The flow rate and hydraulic force can be calculated as

$$q_1 = -q_{\text{orifice}} - \frac{dV}{dx} v, \tag{13}$$

$$q_2 = q_{\text{orifice}} + \frac{dV}{dx} v, \tag{14}$$

$$F = (p_2 - p_1) \frac{\pi}{4} d_a^2, \tag{15}$$

$$d_a = d_b \sin \alpha, \tag{16}$$

$$\alpha = \frac{\pi}{2} - \theta, \tag{17}$$

where q_{orifice} is the volume flow rate of fuel under a difference in pressure, d_a is the active diameter, θ is the semi-angle of the seat, d_b is the diameter of the ball, x is the lift of the poppet, v is its velocity, and $V(x)$ is the increase in the volume of the fluid subject to the throat pressure at the lift of x . The active diameter d_a is shown in Fig. 2(a). The active area is the curved surface of a truncated cone, as shown by the red line in Fig. 2(a). It is assumed that this surface divides the region occupied by the fluid into two. One of these regions is subjected to pressure p_1 and the other to pressure p_2 . q_1 and q_2 are the volume flow rates on the poppet and seat sides, respectively, and $V(x)$ can be calculated as follows:

$$V(x) = \pi x \left[\frac{d_a^2}{4} + x \sin \alpha \cos \alpha \left(\frac{d_a}{2} + \frac{x \sin \alpha \cos \alpha}{3} \right) \right]. \tag{18}$$

q_{orifice} is calculated by using the method described in Sec. II B 3. The hydraulic diameter is calculated by

$$d_h = 2x \cos \alpha. \tag{19}$$

7. Sub-model of needle valve

Similar to that of the ball valve, the sub-model of the needle valve involves calculating the force balance and the flow rate

$$q_1 = -q_{\text{orifice}} + \frac{\pi}{4} (d_{\text{pop}}^2 - d_c^2) v, \tag{20}$$

$$q_2 = -q_{\text{orifice}} + \frac{\pi}{4} d_c^2 v, \tag{21}$$

$$F = p_2 \frac{\pi}{4} d_c^2 + \bar{p} \times \frac{\pi}{4} (d_{\text{pop}}^2 - d_c^2), \tag{22}$$

$$\bar{p} = \frac{p_1 + p_2}{2} \left(1 - e^{-\frac{3x}{\text{taux}}} \right), \tag{23}$$

where d_{pop} , d_c , \bar{p} , x , and taux are the diameter of the poppet, diameter of the cone, average pressure, life of the poppet, and an auxiliary parameter, respectively, as shown in Fig. 2(b). q_{orifice} is calculated using the method described in the sub-model of the orifice. During the calculation of q_{orifice} , the flow area A in Eq. (6) is obtained as follows:²⁴

$$A = \min(A_1, A_2), \tag{24}$$

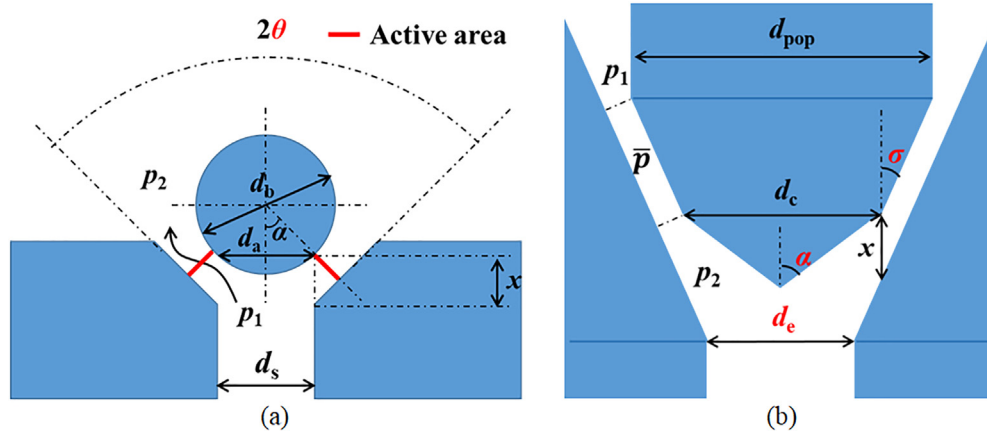


FIG. 2. Ball valve and needle valve: (a) ball valve and (b) needle valve.

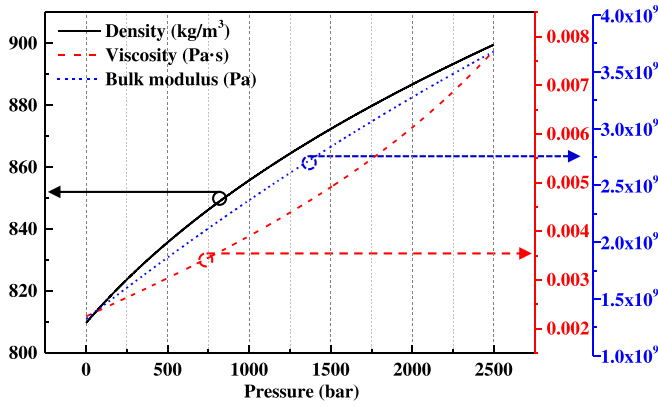


FIG. 3. Variations in density, viscosity, and bulk modulus at 40 °C.

$$A_1 = \pi x \sin \sigma \frac{d_c + x \sin \sigma (\cos \sigma - \sin \sigma \tan \beta_1)}{\cos \beta_1}, \quad (25)$$

$$\tan \beta_1 = M_1 - \sqrt{|M_1^2 - 0.5|}, \quad (26)$$

$$M_1 = \frac{1}{4} \left[\frac{d_c}{x} \left(1 + \frac{1}{(\tan \sigma)^2} \right) + \frac{1}{\tan \sigma} \right], \quad (27)$$

$$A_2 = \pi (x \sin \alpha + m') \varepsilon \frac{d_e - (x \sin \alpha + m') (\cos \alpha + \sin \alpha \tan \beta_2)}{\cos \beta_2}, \quad (28)$$

$$\tan \beta_2 = M_2 - \sqrt{|M_2^2 - 0.5|}, \quad (29)$$

$$M_2 = \frac{1}{4} \left[\frac{d_c \sin \alpha}{x \sin \alpha + m'} \left(1 + \frac{1}{(\tan \alpha)^2} \right) - \frac{1}{\tan \alpha} \right], \quad (30)$$

$$m' = (d_c - d_e) \cos \alpha \frac{\tan \alpha - \tan \sigma}{2 \tan \alpha}, \quad (31)$$

where d_e is the diameter of the hole; α is the half-angle of the seat of the needle valve; σ is the half-angle of its cone; β_1 , β_2 , M_1 , M_2 , and m' are all auxiliary parameters; and the hydraulic diameter d_h is calculated by

$$d_h = 2x \sin \alpha. \quad (32)$$

The related parameter values are listed in Table I.

8. Sub-model of fluid properties

The physical properties of oil ISO4113 are used here. As shown in Fig. 3, the density, bulk modulus, and dynamic viscosity of the fuel all increase with the pressure.

C. Boundary and initial conditions

The boundary conditions of the electromagnetic force are shown in Fig. 4. They were processed based on the signal of the test rig. The pressure source (simulating the rail) was fixed as rail pressure for the entire period of injection. The pressure of the outlet of the return fuel and outlet of the nozzle was set to zero (gauge pressure). These boundary conditions are shown in Fig. 5.

The pressure in the control volume, chamber 1, chamber 3, chamber 5, and chamber 6, was equal to the rail pressure as initial condition.

D. Numerical procedure

As shown in Fig. 5, each sub-model described in Sec. II B was integrated according to the relevant physical connections, which is demonstrated in Fig. 1. From the perspective of modeling, the flow rate (q), force (F), displacement (x), and pressure (Pa) are four key parameters to couple each sub-models. For example, the viscous force calculated by the leakage sub-model [Eq. (12)] was an input to the mechanical sub-model (M_2). The displacement calculated by M_2 [Eq. (1)] was regarded as the displacement of the poppet in Eq. (23). To be clear, the force and displacement are marked in blue and red, respectively. At each instant, the implicit iterative method was applied to numerically solve the equations formed by each element. Due to the non-linearity of the equations, the under-relaxation factor was needed during the iteration process. In particular for the 1D model of the pipeline, the explicit second-order MacCormack method was used.

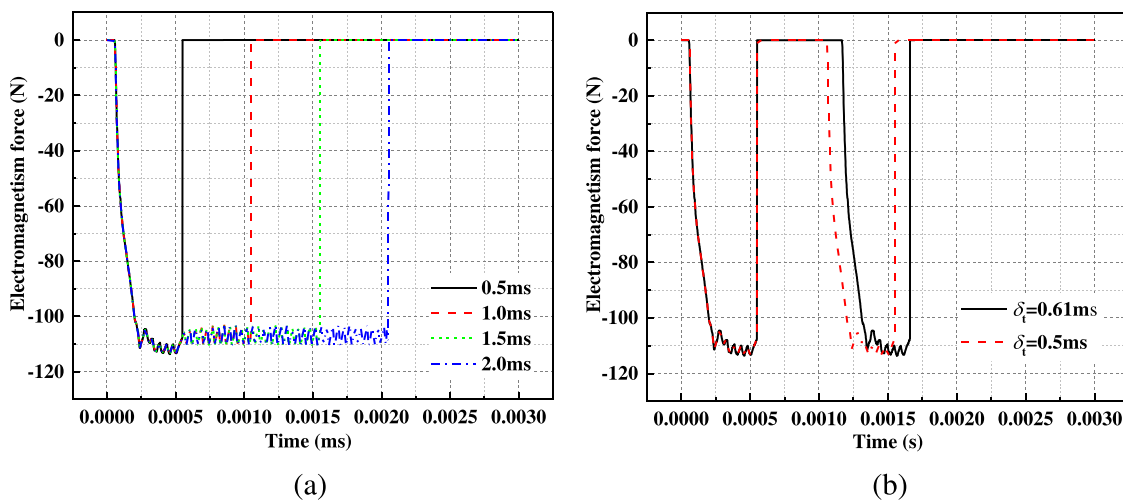


FIG. 4. Electromagnetic force signals: (a) electromagnetic forces with different energizing times and (b) electromagnetic force in the case of multiple injections.

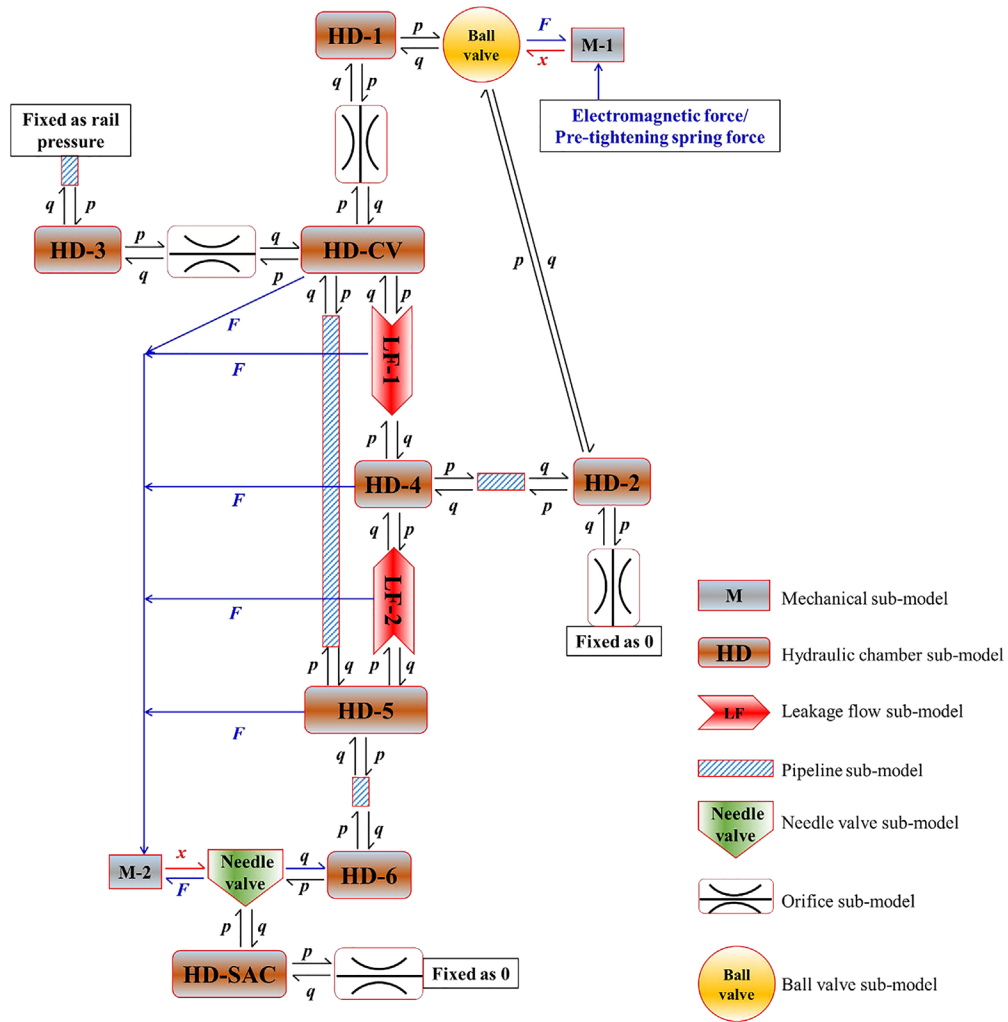


FIG. 5. Network of 1D hydro-mechanical system model of injector.

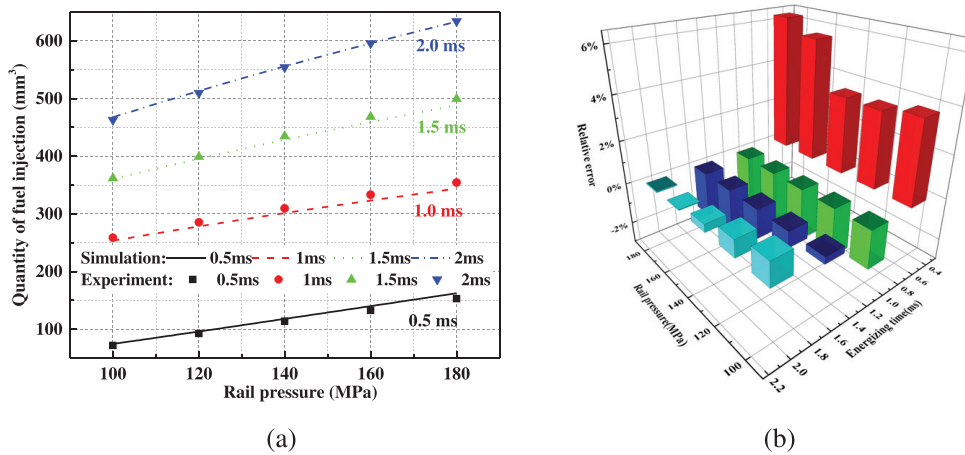


FIG. 6. Model validation: (a) comparison of injected quantities and (b) relative error.

III. RESULTS AND DISCUSSION

A. Model validation

The simulated quantity of fuel injected was compared with experimental data tested on a commercial fuel injector bench, as shown in

Fig. 6(a). The predicted total injected quantity is in good agreement with the experimental data within ranges of the rail pressure of 100–180 MPa and energizing times of 0.5–2.0 ms. The bar representing the relative error in Fig. 6(b) shows that except at a high rail pressure and low energizing time, the relative error of the simulation is lower than 4%.

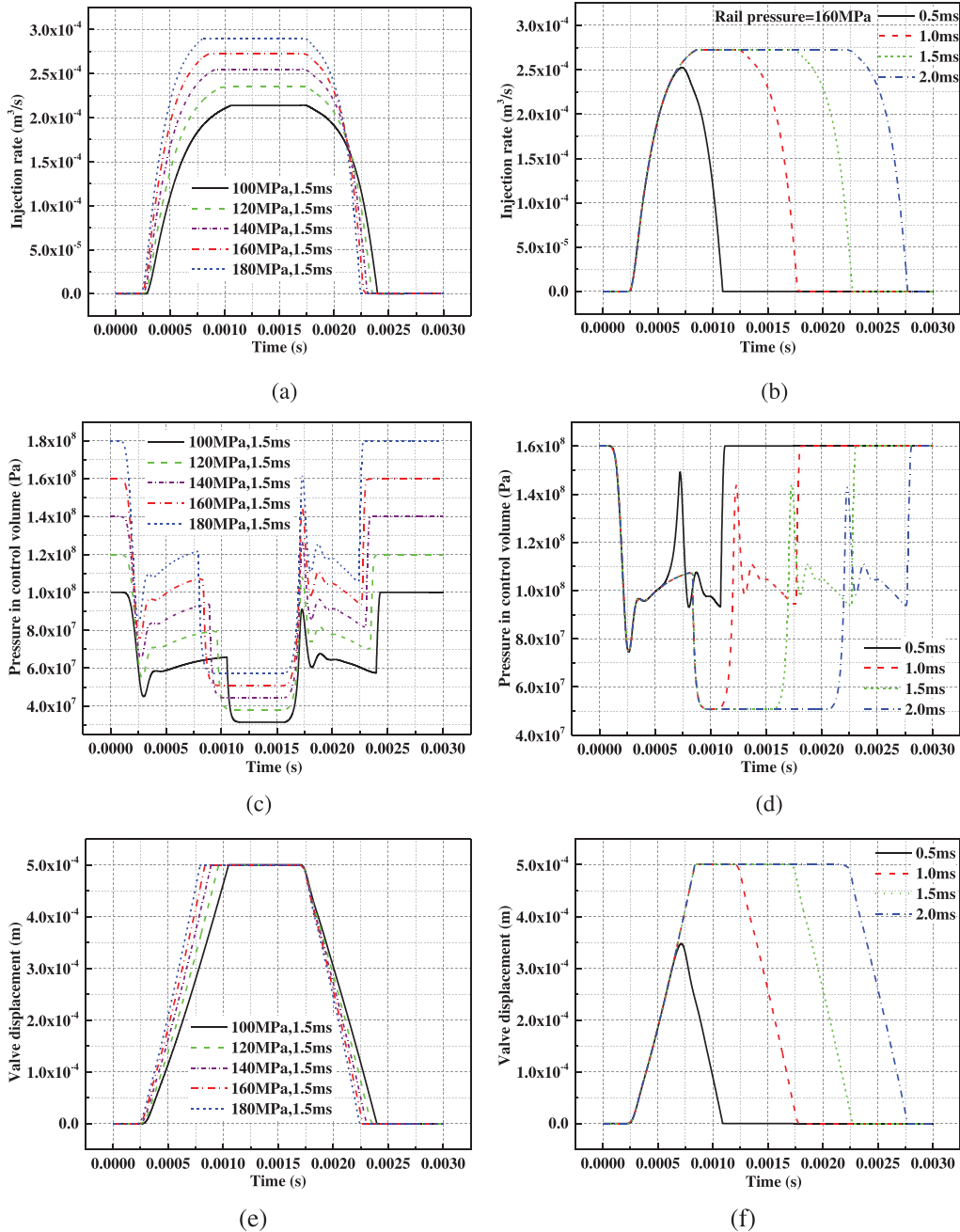


FIG. 7. Rate of injection, pressure in the control volume, and displacement of the needle valve under different injection pressures and energizing times: (a) injection rates under different rail pressures, (b) injection rates under different energizing times, (c) pressure values in CV under different rail pressures, (d) pressure values in CV under different energizing times, (e) displacements of the needle valve under different rail pressure, and (f) displacements of the needle valve under different energizing times.

B. Effects of rail pressure and energizing time

As shown by the curve of the rate of injection in Fig. 7(a), different rail pressures or injection pressures led to different dynamic behaviors under the same energizing time (1.5 ms). With the increase in the rail pressure, the opening and closing delays of the injector decreased. Figures 7(c) and 7(e) show that the pressure of the control volume and movement of the needle had faster responses under a high rail pressure due to an increase in the hydraulic pressure acting on the body of the valve. The maximum rate of injection increased with the rail pressure. This demonstrates that a high rail pressure is beneficial for a large volume of quantity or high-power condition.

In cases where the rail pressure was the same (160 MPa), similar trends of opening and closing were observed, as shown in Fig. 7(b). Figures 7(b), 7(d), and 7(e) show that with an increase in the energizing time, the curve in the closing phase maintained its shape and was translated backward. When the energizing time was too short (e.g., 0.5 ms), the needle could not be raised completely and there was no plateau in the curve of the rate of injection.

C. Effect of geometric parameters (near valve)

Our simulation shows that the following geometric parameters (near valve) have a significant effect on the rate of injection: semi-

angle of the seat of ball valve, diameter of the hole of needle valve, half-angle of seat of the needle valve, and cone half-angle of the needle valve. They are described below.

1. Semi-angle of seat of ball valve

Figure 8 represents the effects of θ values. Figure 8(a) shows that a smaller θ led to quicker opening of the valve for injection. Equations (14) and (15) show that a smaller θ implied a larger active diameter d_a . As a result, hydraulic pressure acting on the body of the valve increased [Eq. (13)]. $V(x)$ was affected at the same time. Under the combined effect of these two factors, the ball valve moved faster as shown in Fig. 8(b). Then, the response of the pressure and movement of the needle quickened, as shown in Figs. 8(c) and 8(d), respectively.

2. Geometric parameters of needle valve

Figure 9 shows the effects of the parameters of the needle valve. Figure 9(a) shows the rate of injection under different diameters d_e of the hole. With the increase in d_e , the rate of injection increased mainly due to an increase in the flow area, as shown in Fig. 9(b), while the lift of the needle was almost the same. In other

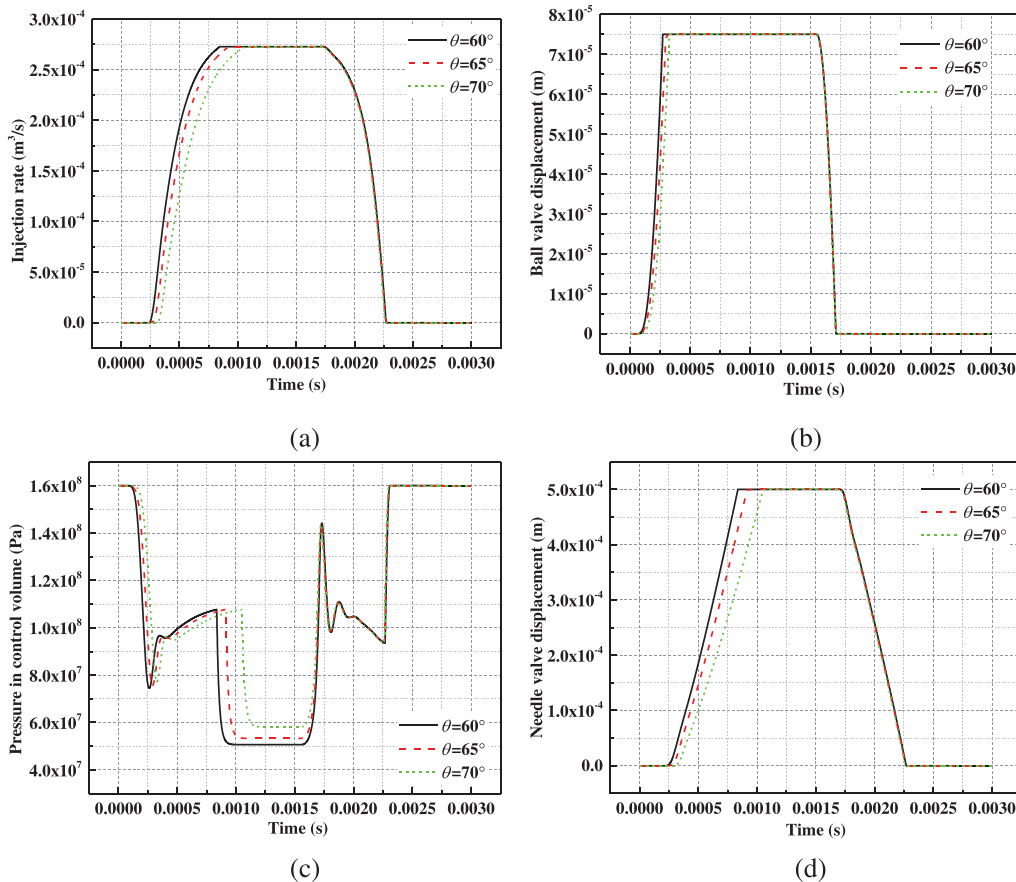


FIG. 8. Effects of semi-angle of the seat of the ball valve θ : (a) injection rate, (b) displacement of ball valve, (c) pressure in control volume, and (d) displacement of needle valve.

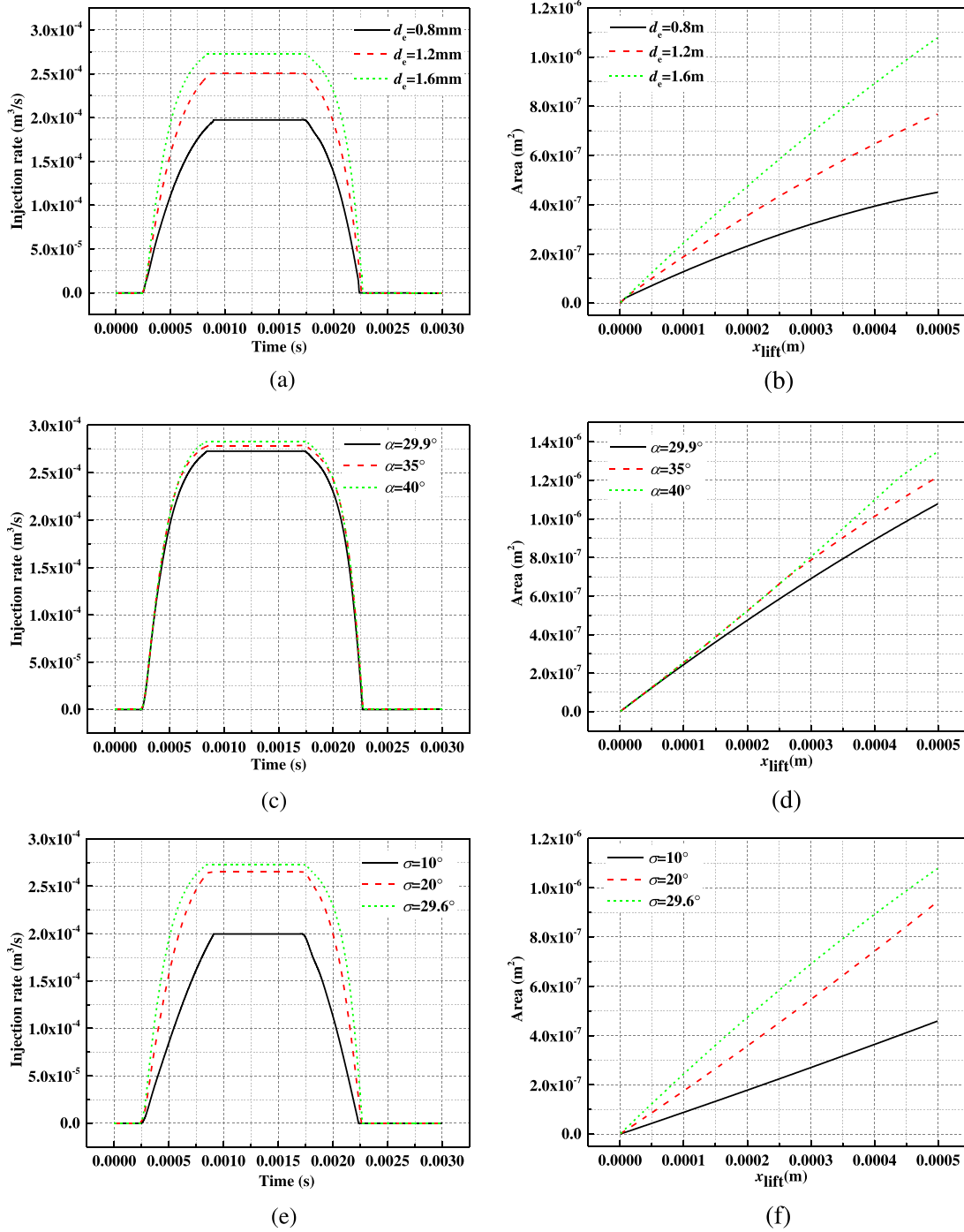


FIG. 9. Effects of d_e , α , and σ of the needle valve: (a) injection rates under different d_e , (b) flow areas of needle valve under different value of d_e , (c) injection rates under different values of α , (d) flow areas of needle valve under different values of α , (e) injection rates under different values of σ , and (f) flow areas of needle valve under different values of σ .

words, the assembly of the needle valve with a larger hole d_e resulted in a larger area of flow under the same displacement of the needle. Similarly, the half-angle of the seat of the needle valve σ and half-angle of the needle cone α had the same effect on the area of

flow, as shown in Figs. 9(d) and 9(f), respectively. This was also true of the rate of injection, as shown in Figs. 9(c) and 9(e). All three parameters were positively correlated with the rate of injection.

D. Dwell time in multi-injection scenario

The critical dwell times under different rail pressures and energizing times are detailed in this section, and the results are provided in Fig. 10. We considered signals of the electromagnetic force in the case of multiple injections. Figures 10(a)–10(c) show the results for two dwell times, $\delta_t = 0.61$ ms and $\delta_t = 0.5$ ms. Under $\delta_t = 0.5$ ms, the first and second injections overlapped, which made it impossible to distinguish between injection events. There was a critical dwell time required to obtain independent injections, as shown in Fig. 10(d). The critical dwell time increased with the rail pressure under an energizing time of 0.5 ms, while the results were different under energizing times of 1.0, 1.5, and 2.0 ms. This is because the needle valve was not fully open under an energizing time of 0.5 ms, and the lower the rail pressure was, the lower was the degree to which the valve opened. As a result, a shorter time was needed for the needle to recover its position in the case of lower rail pressure. However, under a high rail pressure,

there was a plateau in the injection process, and a higher rail pressure implied the faster dynamics of the needle. A higher rail pressure thus led to a shorter critical dwell time.

E. Comparison of pipeline sub-models

Although all four pipelines in the injector could convert the lumped parameter model into a 1D model, only the modification of pipeline 1 (in Fig. 1) had a significant impact on the results. This is because pipelines 2–4 were too short, and the lumped parameter is sufficient to characterize variations in pressure in them. Figure 11(a) shows curves of the rate of injection calculated by using different pipeline models (for pipeline 1). Fuel injection started and ended in both models at the same time. In the 1D model, the rate of injection fluctuated after the needle valve had been opened to the maximum lift. By contrast, the lumped parameter model could not reflect this variation because it ignored the inertia and compressibility of the fluid. Figure 11(b) shows

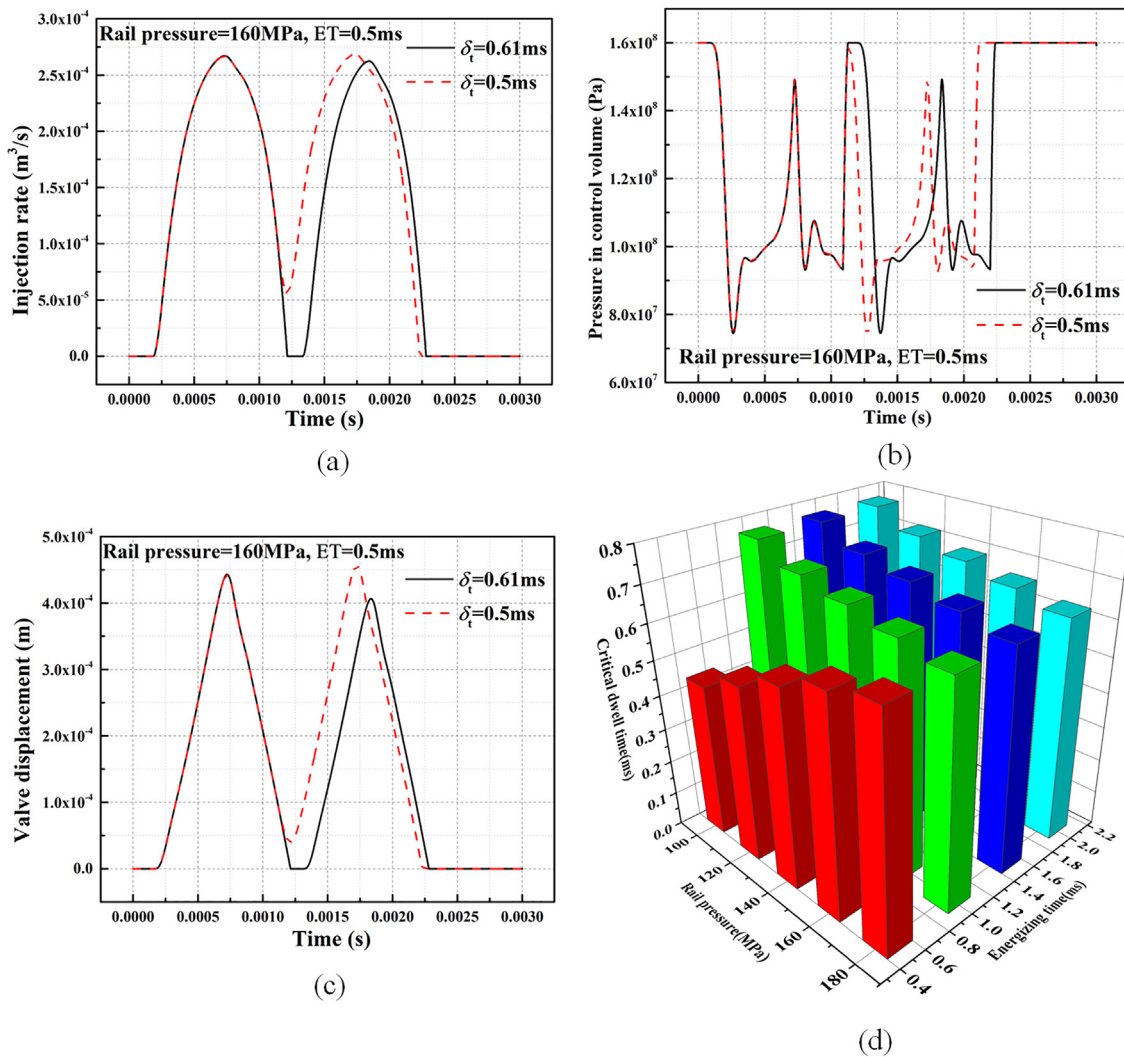


FIG. 10. Multi-injection scenario: (a) injection rate, (b) pressure in control volume, (c) displacement of the valve of the needle, and (d) critical dwell time.

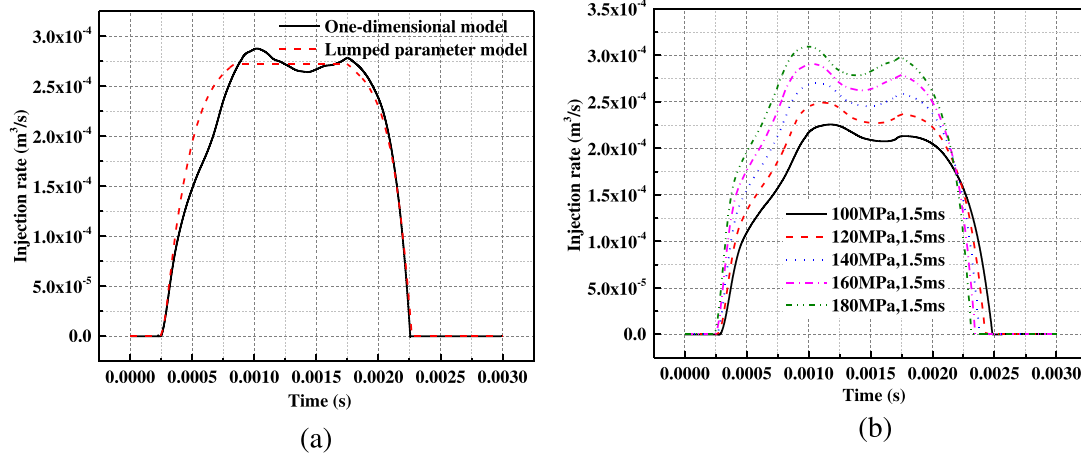


FIG. 11. Results obtained using 1D sub-models of the pipeline: (a) comparison of rates of injection calculated using different pipeline models and (b) injection rates under different rail pressures.

the rates of injection under different rail pressures, calculated by using a 1D sub-model of the pipeline. When the rail pressure was high, the rate of fuel injection increased rapidly at the beginning and decreased rapidly at the end, which is consistent with the previous conclusion in Sec. III B. Similarly, the results described in Secs. III B–III D were valid when the model of the pipeline was altered. In other words, only the shape of the curve changed while the previous qualitative conclusion remained valid.

IV. CONCLUSIONS

In this study, we developed a 1D model of a fuel injector system and the code for it. Numerical results of the rate of fuel injection were validated against experimental results under different rail pressures and energizing times. The main findings are as follows:

- (i) With the increase in the rail pressure, the opening and closing delays of the injector decrease. Too short an energizing time causes the needle to fail to lift to a fully open position.
- (ii) A smaller semi-angle of the seat of the ball valve may lead to a faster opening for injection.
- (iii) The diameter of the hole, half-angle of the seat, and cone half-angle of the needle valve all have positive effects on the rate of injection.
- (iv) The critical dwell time increase with the rail pressure under a short energizing time (0.5 ms), while it decrease with the rail pressure in case of a long energizing time.

ACKNOWLEDGMENTS

This study was supported by the Foundation for Innovative Research Groups of the National Natural Science Foundation of China (No. 51721004), the Basic Research Project of Shaanxi Province (Grant No. 2019ZDXM3–01), and the 111 Project (No. B16038).

AUTHOR DECLARATIONS

Conflict of Interest

The authors have no conflicts to disclose.

DATA AVAILABILITY

The data that support the findings of this study are available from the corresponding author upon reasonable request.

REFERENCES

- ¹F. Y. Li and Q. Z. Lin, “Radial development of pentanol-biodiesel fuel spray in a high-pressure common-rail system,” *Phys. Fluids* **33**, 095115 (2021).
- ²Y. Liu, J. Tian, Z. Song, F. Li, W. Zhou, and Q. Lin, “Spray characteristics of diesel, biodiesel, polyoxymethylene dimethyl ethers blends and prediction of spray tip penetration using artificial neural network,” *Phys. Fluids* **34**, 015117 (2022).
- ³A. Oamjee and R. Sadanandan, “Effects of fuel injection angle on mixing performance of scramjet pylon-cavity flameholder,” *Phys. Fluids* **32**, 116108 (2020).
- ⁴F. Duronio, S. Ranieri, A. D. Mascio, and A. D. Vita, “Simulation of high pressure, direct injection processes of gaseous fuels by a density-based OpenFOAM solver,” *Phys. Fluids* **33**, 066104 (2021).
- ⁵Y. D. Pogulyaev, R. M. Baitimerov, and Y. V. Rozhdstvenskii, “Detailed dynamic modeling of common rail piezo injector,” *Procedia Eng.* **129**, 93 (2015).
- ⁶K. Zhang, X. Huang, Z. Xie, and M. Zhou, “Design and optimization of a novel electrically controlled high pressure fuel injection system for heavy fuel aircraft piston engine,” *Chin. J. Aeronaut.* **31**, 1920 (2018).
- ⁷H. P. Wang, D. Zheng, and Y. Tian, “High pressure common rail injection system modeling and control,” *ISA Trans.* **63**, 265 (2016).
- ⁸S. Patil and S. Sahu, “Air swirl effect on spray characteristics and droplet dispersion in a twin-jet crossflow airblast injector,” *Phys. Fluids* **33**, 073314 (2021).
- ⁹B. A. Reid, G. K. Hargrave, C. P. Garner, and G. Wigley, “An investigation of string cavitation in a true-scale fuel injector flow geometry at high pressure,” *Phys. Fluids* **22**, 031703 (2010).
- ¹⁰L. Tan, X. He, G. Xiao, M. Jiang, and Y. Yuan, “Design and energy analysis of novel hydraulic regenerative potential energy systems,” *Energy* **249**, 123780 (2022).
- ¹¹Y. Wu, M. Li, J. Yin, S. Liu, and T. Lu, “Hydrostatic pressure and interfacial tension induce mode instability in wave propagation along a liquid-filled microtube,” *Phys. Fluids* **32**, 031901 (2020).
- ¹²R. Rahim, R. Mamat, M. Y. Taib, and A. A. Abdullah, “Influence of fuel temperature on a diesel engine performance operating with biodiesel blended,” *J. Mech. Eng. Sci.* **2**, 226 (2012).
- ¹³A. J. Rowane, V. Mahesh Babu, H. B. Rokni, J. D. Moore, M. Gavaises, M. Wensing, A. Gupta, and M. A. McHugh, “Effect of composition, temperature, and pressure on the viscosities and densities of three diesel fuels,” *J. Chem. Eng. Data* **64**, 5529 (2019).

- ¹⁴J. Safarov, U. Ashurova, B. Ahmadov, E. Abdullayev, A. Shahverdiyev, and E. Hassel, "Thermophysical properties of diesel fuel over a wide range of temperatures and pressures," *Fuel* **216**, 870 (2018).
- ¹⁵H. B. Rokni, A. Gupta, J. D. Moore, M. A. McHugh, B. A. Bamgbade, and M. Gavaises, "Purely predictive method for density, compressibility, and expansivity for hydrocarbon mixtures and diesel and jet fuels up to high temperatures and pressures," *Fuel* **236**, 1377 (2019).
- ¹⁶J. Kim, J. Lee, and K. Kim, "Numerical study on the effects of fuel viscosity and density on the injection rate performance of a solenoid diesel injector based on AMESim," *Fuel* **256**, 115912 (2019).
- ¹⁷F. J. Salvador, J. Gimeno, J. Martín, and M. Carreres, "Thermal effects on the diesel injector performance through adiabatic 1D modelling. Part I: Model description and assessment of the adiabatic flow hypothesis," *Fuel* **260**, 116348 (2020).
- ¹⁸R. Payri, F. J. Salvador, M. Carreres, and M. Belmar-Gil, "Thermal effects on the diesel injector performance through adiabatic 1D modelling. Part II: Model validation, results of the simulations and discussion," *Fuel* **260**, 115663 (2020).
- ¹⁹F. J. Salvador, J. Gimeno, J. De la Morena, and M. Carreres, "Using one-dimensional modeling to analyze the influence of the use of biodiesels on the dynamic behavior of solenoid-operated injectors in common rail systems: Results of the simulations and discussion," *Energy Convers. Manage.* **54**, 122 (2012).
- ²⁰N. Hu, J. Yang, P. Zhou, and Y. Hu, "Study of the impact of structural parameters on the dynamic response of an electronic fuel injector," *Energy Convers. Manage.* **136**, 202 (2017).
- ²¹Y. Bai, L. Y. Fan, X. Z. Ma, H. L. Peng, and E. Z. Song, "Effect of injector parameters on the injection quantity of common rail injection system for diesel engines," *Int. J. Automot. Technol.* **17**, 567 (2016).
- ²²G. M. Bianchi, S. Falfari, M. Parotto, and G. Osbat, "Advanced modeling of common rail injector dynamics and comparison with experiments," SAE Paper No. 2003-01-0006, 2003.
- ²³I. Idel'Chik, *Handbook of Hydraulic Resistances* (Mashinostroenie, Moscow, 1975) (in Russian).
- ²⁴L. Fan, Y. Bai, X. Ma, and E. Song, "Analysis upon fuel injection quantity variation of common rail system for diesel engines," *J. Mech. Sci. Technol.* **30**, 3365 (2016).